

# SAGGING AND HOGGING STRENGTHENING OF CONTINUOUS RC BEAMS USING CFRP SHEETS

by

**S. A. El-Refaie, A. F. Ashour and S. W. Garrity**

## ABSTRACT

This paper reports the testing of eleven reinforced concrete two-span beams strengthened in flexure with externally bonded carbon fiber reinforced polymer (CFRP) sheets. The beams were classified into two groups according to the arrangement of the internal steel reinforcement. Each group included one unstrengthened control beam. The main parameters studied were the position, length and number of CFRP layers. External strengthening using CFRP sheets was found to increase the beam load capacity. However, all strengthened beams exhibited less ductility compared with the unstrengthened control beams and showed undesirable sudden failure modes. There was an optimum number of CFRP layers beyond which there was no further enhancement in the beam capacity. Extending the CFRP sheet length to cover the entire hogging or sagging zones did not prevent peeling failure of the CFRP sheets which was the dominant failure mode of beams tested.

**Keywords:** CFRP sheets, reinforced concrete, continuous beams, strengthening, deflection, capacity, reaction, strains, moment redistribution, ductility.

## INTRODUCTION

Although many reinforced concrete beams are of continuous construction, little experimental work on the repair and strengthening on such beams has been reported

(Sharma, 1992, Arduini et al., 1997, Khalifa et al., 1999, Grace et al., 1999, Tann and Delpak, 2000 and El-Refaie et al., 2001). Khalifa et al. (1999) tested nine two-span reinforced concrete beams strengthened with different arrangements of CFRP sheets. All beams were heavily reinforced in flexure to promote shear failure. It was concluded that wrapping the entire beam span using U-shape CFRP sheets was more effective in increasing the beam load capacity than using U-shape CFRP strips. They also found that the smaller the internal shear reinforcement, the higher the efficiency of the external CFRP composite in increasing the beam load capacity. Although the failure mode of the strengthened beams were found to be varied from brittle debonding of the CFRP composite to flexural failure, the load capacity of all strengthened beams was higher than that of the unstrengthened control beam. El-Refaie et al. (2001) presented results of the testing of five reinforced concrete continuous beams strengthened with CFRP laminates; one control beam, three beams strengthened with different arrangements of CFRP plates and one strengthened using CFRP sheets. In all the beams tested, the main longitudinal top steel bars over the central support were the same as those provided at the mid-span soffit. It was concluded that the beam load capacity was increased by up to 55%; however, the ductility of the strengthened beams was reduced. It was also observed that the performance of the beams strengthened with CFRP plates or sheets of equivalent strength was similar.

This paper summarises the testing of eleven two-span beams strengthened with different arrangements of CFRP sheets. Unlike the steel reinforcement of the beams tested in the first phase (El-Refaie et al., 2001), either the top or bottom main longitudinal steel reinforcement was designed to represent beams in need of repair. The influence of position, length and number of CFRP layers on the flexural behaviour of continuous beams was investigated. Different failure modes of strengthened beams tested were

observed such as tensile rupture of the CFRP sheets, CFRP sheet separation and peeling failure of the concrete cover adjacent to the CFRP sheets.

## RESEARCH SIGNIFICANCE

Although a great deal of research has been carried out on simply supported beams strengthened with CFRP composites, little work has been focused on continuous beams. The main aim of this paper is to investigate the efficiency of using CFRP sheets for strengthening of continuous beams. Two measures are used to assess the capacity enhancement of the strengthened beams, namely the ultimate load and moment enhancement ratios. While these two values are always the same for simply supported beams, it will be shown that they are different in the case of strengthened continuous beams.

## TEST PROGRAMME

Beam geometry and reinforcement as well as the loading and support arrangements are illustrated in Figure 1. Each beam was 8500mm long x 150mm wide x 250mm deep. The test specimens were classified into two groups according to the arrangement of the longitudinal steel reinforcement: group H was reinforced with 2 bars of 8mm diameter on the top side of the beam and 2 bars of 20mm diameter on the bottom side, whereas group S was reinforced with an opposite arrangement of the internal longitudinal steel reinforcement as shown in Figure 1 and Table 1. The transverse shear links were 6mm diameter bars at 100mm centres designed to prevent shear failure. The arrangement of the steel reinforcement in groups H and S was designed to promote hogging and sagging flexural failures, respectively, and to represent beams that need repair to compensate the insufficient internal steel reinforcement.

## STRENGTHENING PROCESS

The position, length and number of CFRP layers were the main parameters investigated as summarised in Table 1. The width of the sheets was 110mm and each sheet thickness was 0.117mm; the effective area of CFRP was 12.87 $mm^2$/sheet and the total area of CFRP sheets used in test specimens is given in Table 4. The sheets applied to the top face of the beams were placed symmetrically about the central support. Those applied to the bottom face of the beam were positioned symmetrically about the centres of both spans. Beams H1 and S1 had no external reinforcement and were used as control specimens.

The concrete substrate was initially roughened by sand blasting. Then, it was vacuum cleaned to remove any dust or loose particles from the concrete surface and to expose the aggregates. A 300mm straight edge was used to check that the surface deviation was within the acceptable 1mm limit recommended by the manufacturer.

Two-component epoxy resin primer was prepared in accordance with the manufacturer's recommendations and applied to the concrete substrate by a brush. When the primer had dried to a "touch dry" state, two-component epoxy resin bonding adhesive was prepared in accordance with the manufacturer's recommendations and applied by a brush over the touch-dry primer. The first layer of the CFRP sheets was then placed by hand and pressed onto the adhesive with a rubber roller. Another layer of adhesive was applied over the CFRP sheet and was pressed using a squeegee. Additional CFRP layers were applied by the same way onto the uncured wet adhesive. The complete application was subsequently left to cure for at least 7 days before testing. The bottom face CFRP sheets were applied with the beams turned upside down.

## MATERIAL PROPERTIES

The beams were made from Ordinary Portland cement with a 10mm maximum aggregate size and a target 28 day compressive strength of 30 N/mm². Three 100mm cubes, three 150mm dia. × 300mm high cylinders and three 100x100x500mm prisms were made from each batch of concrete used to make the test beams. The cubes, cylinders and prisms were tested on the same day as the test beams to provide values of the cube strength, $f_{cu}$, splitting tensile strength, $f_{tu}$, and modulus of rupture, $f_r$. The average values of $f_{cu}$, $f_{tu}$ and $f_r$ are given in Table 1. The yield strength, $f_y$, ultimate strength, $f_u$, and modulus of elasticity, $E_s$, of the internal steel reinforcement used in the test specimens are given in Table 2. The unidirectional CFRP sheets and epoxy bonding adhesive were provided by Weber and Broutin (UK) Ltd; details of the mechanical properties of these materials, obtained from the manufacturer's data sheets, are summarised in Table 3.

## TEST RIG AND RESULTS

Each test beam, which comprised two equal spans of 3830mm each, was loaded as shown in Figure 1. Load cells were used to measure the end support reactions and electrical resistance strain (ERS) gauges were attached to the longitudinal steel bars and CFRP sheets at the bottom mid-spans and the top over the central support to measure surface strains. The mid-span deflections were measured using linear variable differential transformers (LVDTs). Load cell, ERS gauge and LVDT readings were recorded automatically, at each load increment (10 kN), using data logging equipment.

### *Crack propagation before failure*

In all cases, the provision of CFRP sheets resulted in improved crack control when compared with the unstrengthened control beams. It was noticed in some strengthened beams that the cracks initiated away from the extreme tension fiber of the concrete

adjacent to the external CFRP composite as a result of the high restraining action to the crack initiation provided by the CFRP composite placed immediately at the extreme tension fiber of the concrete. However, it should be mentioned that beam H6 which was strengthened over the central support and on the beam soffit exhibited the largest number of cracks before failure of all the beams in group H. Beams H5 and S3 exhibited wide long flexural cracks just next to the CFRP sheet ends (the ends near the end supports in beam S3) at 30% and 75% of each beam failure load, respectively.

***Failure modes***

Three different failure modes were observed in the tests and are described below. Table 4 gives the mode of failure for each beam.

**Mode 1: Conventional ductile flexural failure**

This occurred due to yielding of the internal tensile steel reinforcement followed by concrete crushing at both the central support and mid-span sections for control beams H1 and S1. Hogging flexural failure of control beam H1 was observed as a result of yielding of the tensile steel reinforcement at the central support earlier than that at the beam mid-spans. Conversely, sagging flexural failure of control beam S1 occurred as a result of yielding of the tensile steel reinforcement at the beam mid-spans earlier than that at the central support as shown in Figure 2. A major diagonal crack occured close to the central support due to the combination of high shear and moment at this region as shown in Figure 2(b).

**Mode 2: Tensile rupture of the CFRP sheets**

Beams H2 (see Figure 3) and H6 exhibited tensile rupture of the CFRP sheets over the central support at 80% and 70% of each beam failure load, respectively. Tensile rupture of the CFRP sheets was followed by flexural failure in beam H2 and by peeling failure of the concrete cover attached to the soffit sheets in beam H6 (Figure 4). Rupture of the CFRP

sheets was sudden and accompanied by a loud noise indicating a rapid release of energy and a total loss of load capacity.

**Mode 3: Peeling failure**

This type of failure usually occurred in the concrete cover along the steel reinforcement level adjacent to the external CFRP composite, for a large number of strengthened beams in the test programme as shown in Figures 4 to 7 and indicated in Table 4. It was sudden, explosive, accompanied with a loud noise and resulted in immediate beam failure. In general, peeling failure of the concrete cover adjacent to the CFRP sheets bonded over the central support was more explosive with a louder noise than that occurred adjacent to the soffit CFRP sheets. Using short CFRP sheets in beams H5 resulted in peeling failure of the concrete cover initiated from the CFRP sheet end as illustrated in Figure 5. Conversely, peeling failure of the concrete cover occurred away from the CFRP sheet end in beams H3 (Figure 6), S4 (Figure 7) and H4. A thin layer of concrete was attached to the separated part of the CFRP sheet at the adjacent zone to the delaminated concrete cover as shown in Figures 6 and 7. Peeling failure of the concrete cover in beam S4 was at the mid-span region on the side near the central support (Figure 7) where there was high shear force. Extending the CFRP sheet to cover the entire hogging zone such as in beam H3 or the entire sagging zone such as in beam S4 did not prevent peeling failure of the concrete cover. In beams S2 and S5, CFRP sheet separation without concrete attached occurred along the adhesive / concrete and CFRP sheet / adhesive interfaces as shown in Figure 8 (beam S2). This may be as a result, in part, of the workmanship problems. It was accompanied by a little noise before beam failure indicating impending failure of the adhesive. Tensile rupture for part of the CFRP sheet width at mid-span of beam S2 was observed at beam failure (Figure 8).

***Beam stiffness and mid-span deflection***

Figure 9 shows the relationship between the total applied load (= $2P$, where $P$ is the mid-span point load) versus the mid-span deflection for group H and S beams. At early stages of loading before concrete cracking, all beams in each group exhibited very similar stiffnesses. After concrete cracking, all strengthened beams exhibited higher stiffnesses and smaller mid-span deflections than those obtained for the corresponding control beams at the same value of the applied load. The stiffnesses of beams H2 and H6 were abruptly decreased after tensile rupture of the CFRP sheets over the central support. Similarly, the stiffness of beam H5 decreased abruptly after the onset of peeling failure at 87% of the beam failure load as shown in Figure 9. The provision of the CFRP sheets on the soffit of beam H6 was found to prevent further decrease in the stiffness resulted from tensile rupture of the CFRP sheets over the central support. Beams in group H were generally stiffer than those in group S as shown in Figure 9. Increasing the length and number of CFRP layers over the central support or on the beam soffit decreased the mid-span deflection and generally increased the stiffness at the same value of the applied load as shown in Figure 9.

***End support reactions***

Figure 10 shows the amount of the load transferred to the end support plotted against the total applied load for group H and S beams. The reaction obtained from an elastic analysis assuming uniform flexural stiffness along the beam span is also plotted in Figure 10. As the results recorded for the two end support reactions were similar, only one end-support reaction is plotted in Figure 10. At the early stages of loading, the end support reactions of all beams tested in each group were very similar and close to that obtained from an elastic analysis. Approaching beam failure and for the same value of the applied load, the end support reaction was less than the elastic reaction due to increasing the length and

number of CFRP layers over the central support as shown in Figure 10. Conversely, at the same value of the applied load, increasing the length and number of CFRP layers bonded to the beam soffit was found to increase the end support reaction as depicted in Figure 10. The end support reactions of beams in group H were larger than those of beams in group S as shown in Figure 10. A sharp increase in the end support reaction was observed in beams H2, H5 and H6 after tensile rupture of the CFRP sheets or onset of peeling failure over the central support earlier before beam failure. This may have resulted from the sudden reduction of the beam flexural stiffness at the central support region due to tensile rupture or peeling of the CFRP sheets. It should be noted that increasing the length and number of CFRP layers to substitute the insufficient internal steel reinforcement resulted in a relatively uniform flexural stiffness along the beam span compared with that of the corresponding control beams. Hence, the end support reactions of the strengthened beams in groups H and S were relatively closer to that calculated from an elastic analysis than those of the respective control beams.

***Internal tensile steel reinforcement strains***

Figures 11 and 12 show the total applied load against the tensile strains in the top steel bars over the central support and bottom steel bars at mid-spans for group H and S beams, respectively. Strains in the top steel bar over the central support of beam S3 are not displayed in Figure 12 because of damage of ERS gauge at that position during compaction of fresh concrete while casting. As designed, the top steel bars over the central support of the control beam H1 yielded earlier than the bottom steel bars at the beam mid-spans, whereas opposite results were noticed for the control beam S1 as indicated in Figures 11 and 12. The total applied load, at which the tensile steel bars of strengthened beams yielded, was increased compared with those of the corresponding control beam.

***CFRP sheet strains***

Figure 13 shows the total applied load plotted against the tensile strains measured at the middle of the CFRP sheets for strengthened beams of groups H and S. The tensile strains of the CFRP sheets increased significantly after concrete cracking and yielding of the internal tensile steel reinforcement. Not only increasing the number of CFRP layers reduced the tensile strains in the CFRP sheets at a given value of the applied load, but it also decreased the maximum tensile strains in the CFRP sheets achieved before beam failure (Figure 13). Increasing the CFRP sheet length increased the maximum tensile strains achieved before beam failure as illustrated in Figure 13 for beams H3, H5, S3 and S4.

Figure 14 gives a comparison between tensile strains in CFRP sheets and the adjacent steel bars at different load levels for beams H2, H6, S4 and S5. At early stages of loading, it can be observed that the strains in CFRP sheets are reasonably close to those in the adjacent steel bars. As expected, strains in CFRP sheets are always higher than those in the adjacent steel bars at the same load level, indicating effective composite action of different materials.

***Failure load and ultimate load enhancement ratio***

The failure load results for all the beams tested are summarised in Table 4. In addition to the total ultimate load, $P_u$ (= $2P$ where $P$ is the mid-span point load), Table 4 also gives the ultimate load enhancement ratio, $\xi$, that is the ratio of the ultimate load of a strengthened beam to that of the corresponding unstrengthened control beam. It should be mentioned that the ultimate load enhancement ratio of a strengthened beam having a concrete compressive strength higher than that of the control beam may be slightly larger than would be the case if the same compressive strength of concrete was used for both beams. Table 4 shows that using CFRP composites for the strengthening of continuous

beams is an effective technique and that the load capacity can be increased by up to a factor of 2, as was the case for beam S4. Equilibrium considerations of two span reinforced concrete beams at ductile flexural failure show that the contribution of the sagging moment to the load capacity is twice as that of the hogging moment (Kong and Evans 1987). In the current tests, the sagging bending capacity of the control beam H is larger than that of the control beam S because of the steel reinforcement details. Therefore, the ultimate load of control beam H1 (138.0 kN) was higher than that of control beam S1 (83.6 kN). This may explain the larger ultimate load enhancement ratio obtained for beam S4 ($\xi$ = 2.04) strengthened on its soffit for nearly the entire sagging zone than that determined for beam H3 ($\xi$ = 1.25) strengthened over the central support for nearly the entire hogging zone. For a specified length of the CFRP sheets, there was an optimum number of CFRP layers beyond which the beam load capacity decreased such as for beams H3 and H4, or at least had not been improved such as for beams S2 and S3 as indicated in Table 4. Increasing the length of the CFRP sheets was found to increase the load capacity of the strengthened beam as found when comparing the results for beams H3 and H5. A similar conclusion can be drawn by comparing the results for beams S3 and S4. However, increasing the CFRP sheet length was not effective when tensile rupture of the sheets occurred. This can be noticed by comparing the load at which tensile rupture of the CFRP sheets occurred over the central support for beams H2 and H6 (121.5 kN for both beams as indicated in Table 4).

***Moment enhancement ratio and load-moment relationship***

Table 5 gives the ultimate moment enhancement ratio, $\eta$, that is the ratio between the ultimate moment of a strengthened section in a strengthened beam and that of the corresponding section in the respective unstrengthened control beam. The bending moment was calculated based on satisfying the equilibrium conditions using the measured

end support reaction and mid-span applied load. All strengthened sections resisted higher moments than the corresponding unstrengthened sections in the respective control beams. By comparing the ultimate load enhancement ratio of a strengthened beam and the moment enhancement ratio of a strengthened section in the same beam, it can be concluded that the latter was significantly higher than the former. Such a conclusion is not valid for simply supported beams strengthened with external reinforcement where the moment and ultimate load enhancement ratios are the same.

Figures 15 and 16 show the total applied load plotted against the hogging and sagging bending moments for group H and S beams, respectively. The hogging and sagging bending moments obtained from an elastic analysis based on assuming uniform flexural stiffness along the beam span are also plotted in Figures 15 and 16. The behaviour of all beams at early load levels was nearly elastic. By increasing the applied load, many cracks occurred, the steel reinforcement yielded and consequently the bending moment was different from that calculated based on an elastic analysis as can be seen from Figures 15 and 16. For beams in group H, the hogging bending moments are always more and the sagging bending moments are always less than the elastic predictions and the reverse is true for beams in group S; the higher the number of CFRP layers used, the closer the bending moment to the elastic predictions as shown in Figures 15 and 16. This may be attributed to the variation of the flexural stiffness along the beam span. In other words, external hogging and sagging CFRP sheets tended to compensate for the insufficient internal steel reinforcement in the unstrengthened control beams H1 and S1 and attracted more moments to their regions. After tensile rupture of the CFRP sheets in beams H2 and H6 and the onset of peeling failure of the CFRP sheets in beam H5, a sharp decrease in the hogging bending moment and a consequent increase in the sagging bending moment were observed (Figure 15).

***Moment redistribution***

The moment redistribution ratio, $\beta$, given in Table 5 was calculated for the sagging bending moment at the beam mid-span and the hogging bending moment at the central support at beam failure. It was calculated from:

$$\beta = \frac{M_m - M_e}{M_e} \times 100\% \quad (1)$$

where $M_m$ is the bending moment from experiments and $M_e$ is the bending moment calculated from elastic analysis. Table 5 shows that the moment redistribution ratio was appreciably dependent on the area and arrangement of the internal steel reinforcement. Where there was a small area of the steel reinforcement on the bottom side of the beam, there was high moment redistribution ratio. For instance, beams S1 and S4 having a small area of the bottom steel reinforcement exhibited higher moment redistribution ratios than those obtained for beams H1 and H3 having an opposite arrangement of the internal steel reinforcement as indicated in Table 5. Increasing the length and number of CFRP layers decreased the moment redistribution ratio such as for beams H2, H3, H4 and H5 in Table 5. Tensile rupture or onset of peeling failure of the CFRP sheets over the central support in beams H2, H5 and H6 before beam failure, resulted in increasing the moment redistribution ratio appreciably at beam failure as shown in Table 5.

***Beam ductility***

Ductility of a structural element can be defined as the ability of the structural element to sustain large deformations before reaching its failure. Few researchers (Mukhopadhyaya et al. (1998)) have developed different indices in an attempt to measure the ductility of simply supported beams strengthened with external reinforcement. As far as the authors are aware, no ductility indices have been proposed for continuous beams strengthened in flexure with external reinforcement. In the following, the deflection ductility index, $\mu_\Delta$, used

for simply supported beams by Mukhopadhyaya et al. (1998) is adopted to measure the ductility of continuous beams tested. The deflection ductility index, $\mu_\Delta$, is defined as:

$$\mu_\Delta = \frac{\Delta_u}{\Delta_y} \quad (2)$$

where $\Delta_u$ is the mid-span deflection at beam ultimate load and $\Delta_y$ is the mid-span deflection at yield load of the tensile steel reinforcement.

The deflection ductility index, $\mu_\Delta$, given in Table 5 was calculated at the lower yielding load of the tensile reinforcement over the central support or the beam mid-span. As can be seen from Table 5, all strengthened beams exhibited less ductility than the corresponding unstrengthened control beams. Only beam H2 showed nearly similar ductility at failure as that of the control beam H1 because both beams failed in flexure at the ultimate load level. However, if the ductility was considered at tensile rupture of the CFRP sheets, beam H2 would have less ductility than that of the control beam H1 as given in Table 5. The deflection ductility index, $\mu_\Delta$, seems to be a good measure of the ductility of the continuous beams tested. For example, increasing the number of CFRP layers was found to decrease the beam ductility due to increasing the stiffening effect attained from increasing the number of CFRP layers such as in beams H2, H3, S2, S3, S4 and S5 (Table 5). Only beam H4 showed higher ductility than beam H3 which had less number of CFRP layers. This may be as a result of earlier yielding of the steel reinforcement over the central support in beam H4 compared with that in beam H3. Beam S5 exhibited no ductility at all ($\mu_\Delta$ = 1.00) due to separation of the CFRP sheets at early load levels.

## CONCLUSIONS

Based on the experimental investigation described in this paper, the following conclusions

are drawn:

- The provision of CFRP external reinforcement was found to increase the strength of continuous reinforced concrete beams. An increase in the load capacity of up to twice that of the unstrengthened control beam was obtained, however this was accompanied by a reduction in ductility and undesirable sudden failure characteristic.
- Increasing the length and number of CFRP layers decreased the mid-span deflection and generally increased the stiffness of the strengthened beam.
- Sudden, undesirable peeling failure of the concrete cover adjacent to the CFRP sheets was the dominant failure mode of the strengthened beams tested. Increasing the CFRP sheet length to cover the entire hogging or sagging zones did not prevent this mode of failure. Further research into the performance of end anchorage techniques is necessary in order to minimise the risk of this mode of failure.
- Increasing the CFRP sheet length was found to be ineffective when tensile rupture of the CFRP sheets was the failure mode.
- Peeling failure of the concrete cover was found to start from the end of the CFRP sheets when short and large number of CFRP layers were used. Conversely, peeling failure of the concrete cover started away from the CFRP sheet end when longer CFRP sheets were used.
- At a particular value of the applied load, increasing the length and number of CFRP layers bonded to the beam soffit increased the end support reaction, whereas increasing the length and number of CFRP layers bonded over the central support decreased the end support reaction.
- The load at which the internal steel reinforcement in a strengthened beam yielded was higher than that of the corresponding steel reinforcement in the unstrengthened control beam.

- The CFRP sheet tensile strains increased significantly after concrete cracking and yielding of the tensile steel reinforcement.
- Unlike simply supported beams, the enhancement in the bending moment capacity of a continuous beam due to external strengthening was found to be higher than that in the load capacity of the continuous beam.

## ACKNOWLEDGEMENT

The first author acknowledges the grant provided from the Egyptian government to fulfil this research. The experimental work described in this paper was conducted in the Heavy Structures Laboratory in the University of Bradford; the assistance of the laboratory staff is acknowledged. The authors are grateful to Weber and Broutin (UK) Ltd. for providing the CFRP reinforcement and the associated priming and bonding materials for the research.

## REFERENCES

1. Arduini, M., Nanni, A., Tommaso, A. D. and Focacci, F. (1997), “Shear response of continuous RC beams strengthened with carbon FRP sheets”, *Non-Metallic (FRP) Reinforcement for Concrete Structures*, Proceedings of the Third International Symposium (FRPRCS-3), Sapporo, Japan, October, Vol. 1, pp. 459-466.
2. Khalifa, A., Tumialan, G., Nanni, A. and Belarbi, A. (1999), “Shear strengthening of continuous reinforced beams using externally bonded carbon fiber reinforced polymer sheets”, *Fourth International Symposium on Fiber Reinforced Polymer Reinforcement for Reinforced Concrete Structures*, American Concrete Institute, pp. 995-1008.
3. Grace, N. F., Soliman, A. K., Abdel-Sayed, G. and Saleh, K. R. (1999), “Strengthening of continuous beams using fiber reinforced polymer laminates”,

*Fourth International Symposium on Fiber Reinforced Polymer Reinforcement for Reinforced Concrete Structures*, American Concrete Institute, pp. 647-657.

4. El-Refaie, S A., Ashour, A F. and Garrity, S W. (2001), "Strengthening of reinforced concrete continuous beams with CFRP composites", *The International Conference on Structural Engineering, Mechanics and Computation*, Cape Town, South Africa, 2-4 April, pp. 1591-1598.
5. Sharma, A. K. (1992), "Tests of reinforced concrete continuous beams repaired with and without fibro-ferrocrete", *Concrete International: Design and Construction*, March, Vol. 14, No. 3, pp. 36-40.
6. Tann, D. B. and Delpak, R. (2000), "Shear strengthening of continuous reinforced concrete beams using externally bonded carbon fiber sheets", *Concrete Communication Conference 2000, The 10th BCA Annual Conference on Higher Education and the Concrete Industry*, 29-30 June, Birmingham, UK, pp. 325-338.
7. Mukhopadhyaya, P., Swamy, R. N. and Lynsdale, C. "Optimizing Structural Response of Beams Strengthened with GFRP Plates", Journal of Composites for Construction, May 1998, pp. 87-95.
8. Kong, F. K. and Evans, R. H. *Reinforced and Prestressed Concrete* , 3rd Ed., Chapman & Hall, London, 1987, 508p.

# NOTATIONS

| | | |
|---|---|---|
| $E_s$ | = | modulus of elasticity of steel reinforcement |
| $f_{cu}$ | = | concrete cube strength |
| $f_r$ | = | modulus of rupture of concrete |
| $f_{tu}$ | = | tensile splitting strength of concrete |
| $f_y$ | = | yield strength of steel reinforcement |
| $f_u$ | = | ultimate strength of steel reinforcement |
| $L_1$ | | length of CFRP sheets over the central support |
| $L_2$ | | length of CFRP sheets at the beam soffit |
| $M_m$ | = | bending moment at beam failure from experiments |
| $M_e$ | = | bending moment calculated from elastic analysis |
| $P$ | = | mid-span point load |
| $P_u$ | = | total ultimate load of test specimens |
| $\xi$ | = | ultimate load enhancement ratio |
| $\eta$ | = | ultimate moment enhancement ratio |
| $\beta$ | = | moment redistribution ratio |
| $\mu_\Delta$ | = | deflection ductility index |
| $\Delta_u$ | = | mid-span deflection at ultimate load |
| $\Delta_y$ | = | mid-span deflection at yield load of the tensile steel reinforcement |

TABLE 1 Details of test specimens

| Group no. | Beam no. | Over the central support sheets | | Sheets at the beam soffit of each span | | Internal steel reinforcement | | | $f_{cu}$ (N/mm$^2$) | $f_{tu}$ (N/mm$^2$) | $f_r$ (N/mm$^2$) |
|---|---|---|---|---|---|---|---|---|---|---|---|
| | | Number of layers | Sheet length $L_1$ (m) | Number of layers | Sheet length $L_2$ (m) | Top | Bottom | Vertical | | | |
| H | H1 | None | None | None | None | 2 bars of 8mm dia.• | 2 bars of 20mm dia.* | 6mm dia links at 100mm centres+ | 24.0 | 1.9 | 3.0 |
| | H2 | 2 | 2.0 | None | None | | | | 43.5 | 3.7 | 4.5 |
| | H3 | 6 | 2.0 | None | None | | | | 33.0 | 2.8 | 3.2 |
| | H4 | 10 | 2.0 | None | None | | | | 33.2 | 2.9 | 3.3 |
| | H5 | 6 | 1.0 | None | None | | | | 46.0 | 4.1 | 5.1 |
| | H6 | 2 | 3.0 | 2 | 1.0 | | | | 44.0 | 3.8 | 4.5 |
| S | S1 | None | None | None | None | 2 bars of 20mm dia.* | 2 bars of 8mm dia.• | | 26.0 | 2.7 | 3.4 |
| | S2 | None | None | 2 | 2.0 | | | | 42.9 | 3.6 | 4.5 |
| | S3 | None | None | 6 | 2.0 | | | | 33.3 | 3.0 | 3.6 |
| | S4 | None | None | 6 | 3.5 | | | | 42.8 | 3.5 | 4.5 |
| | S5 | None | None | 10 | 3.5 | | | | 24.4 | 2.7 | 3.2 |

TABLE 2 Properties of internal steel reinforcing bars

| Bar diameter (mm) | Yield strength, $f_y$ ($N/mm^2$) | Ultimate strength, $f_u$ ($N/mm^2$) | Modulus of elasticity, $E_s$ ($kN/mm^2$) |
|---|---|---|---|
| 6 (plain round mild steel stirrups) | 308 | 355 | 200 |
| 8 (high yield deformed steel bars) | 505 | 605 | 200 |
| 20 (high yield deformed steel bars) | 510 | 615 | 200 |

TABLE 3 Properties of primer, epoxy bonding adhesive and CFRP sheets

| Material property | Epoxy resin primer | Epoxy resin bonding adhesive | CFRP sheets |
|---|---|---|---|
| Compressive strength ($N/mm^2$) | 100 | 80 | N/A |
| Tensile strength ($N/mm^2$) | 19 | 17 | 3900 |
| Young's Modulus ($kN/mm^2$) | 5.0 | 5.0 | 240 |
| Flexural strength ($N/mm^2$) | 30 | 28 | N/A |
| Bond to concrete ($N/mm^2$) | > 5.3 | > 4.0 | N/A |

TABLE 4 Ultimate load ($P_u$) and ultimate load enhancement ratio ($\xi$□)

| Group no. | Beam no. | Size of CFRP | | $P_u$ (kN) | $\xi$ | Failure mode |
|---|---|---|---|---|---|---|
| | | Total area ($mm^2$) | Length (m) | | | |
| H | H1 | None | None | 138.0 | 1.00 | Flexural failure |
| | H2 | 25.74 (Top) | 2.0 (Top) | 152.3 (121.5*) | 1.10 (0.88*) | Tensile rupture of CFRP sheets followed by flexural failure |
| | H3 | 77.22 (Top) | 2.0 (Top) | 172.9 | 1.25 | Peeling failure |
| | H4 | 128.7 (Top) | 2.0 (Top) | 162.6 | 1.18 | Peeling failure |
| | H5 | 77.22 (Top) | 1.0 (Top) | 162.6 (142.0•) | 1.18 (1.03•) | Peeling failure |
| | H6 | 25.74 (Top)<br>25.74 (Bottom) | 3.0 (Top)<br>1.0 (Bottom) | 172.9 (121.5*) | 1.25 (0.88*) | Tensile rupture of top CFRP sheets followed by peeling failure of soffit sheets |
| S | S1 | None | None | 83.6 | 1.00 | Flexural failure |
| | S2 | 25.74 (Bottom) | 2.0 (Bottom) | 121.8 | 1.46 | Separation of CFRP sheets |
| | S3 | 77.22 (Bottom) | 2.0 (Bottom) | 121.8 | 1.46 | Peeling failure |
| | S4 | 77.22 (Bottom) | 3.5 (Bottom) | 170.5 | 2.04 | Peeling failure |
| | S5 | 128.7 (Bottom) | 3.5 (Bottom) | 111.7 | 1.34 | Separation of CFRP sheets |

* Tensile rupture of the CFRP sheets occurred over the central support.

• Onset of peeling failure.

TABLE 5 Ultimate moment enhancement ratio ($\eta$□), moment redistribution ratio ($\beta$□□) at failure and deflection ductility index ($\mu_{\Delta}$)

| Group no. | Beam no. | $\eta$□ | $\beta$% | | $\mu_{\Delta}$ |
|---|---|---|---|---|---|
| | | | Sagging | Hogging | |
| H | H1 | 1.00 | 38.40 | -64.00 | 4.10 |
| | H2 | 1.42 | 32.65 (18.72*) | -54.41 (-31.20*) | 4.34 (1.83*) |
| | H3 | 2.19 | 11.19 | -18.64 | 1.35 |
| | H4 | 2.50 | 6.32 | -10.53 | 1.74 |
| | H5 | 1.65 | 30.05 (18.83•) | -50.08 (-31.37•) | 2.64 (1.23•) |
| | H6 | 1.33 (1.24+) | 36.07 (21.14*) | -60.12 (-35.23*) | 3.46 (1.71*) |
| S | S1 | 1.00 | -52.40 | 87.41 | 12.85 |
| | S2 | 2.04 | -36.70 | 61.14 | 6.21 |
| | S3 | 2.22 | -33.20 | 55.36 | 2.93 |
| | S4 | 3.34 | -27.20 | 45.31 | 2.52 |
| | S5 | 2.55 | -12.40 | 20.59 | 1.00# |

+ Sagging moment enhancement ratio of the strengthened mid-span section.

* Tensile rupture of the CFRP sheets occurred over the central support.

• Onset of peeling failure.

# There is no ductility.

**List of Figure Captions:**



**List of Table Captions:**

**Biographical Sketch:**

**S.A.El-Refaie** is currently a lecturer at Helwan University, Egypt. He obtained his BSc degree from the Department of Civil Engineering, Helwan University, Egypt in 1994 and his PhD from the Department of Civil & Environmental Engineering at the University of Bradford, UK in 2001.

**A.F.Ashour** is currently a lecturer at the University of Bradford, UK. He obtained his BSc and MSc degrees from Mansoura University, Egypt and his PhD from Cambridge University, UK. His research interests include shear, plasticity and optimisation of reinforced concrete and masonry structures.

**S. W. Garrity** is a visiting research fellow at the University of Bradford, UK and the principal of Garrity Associates.

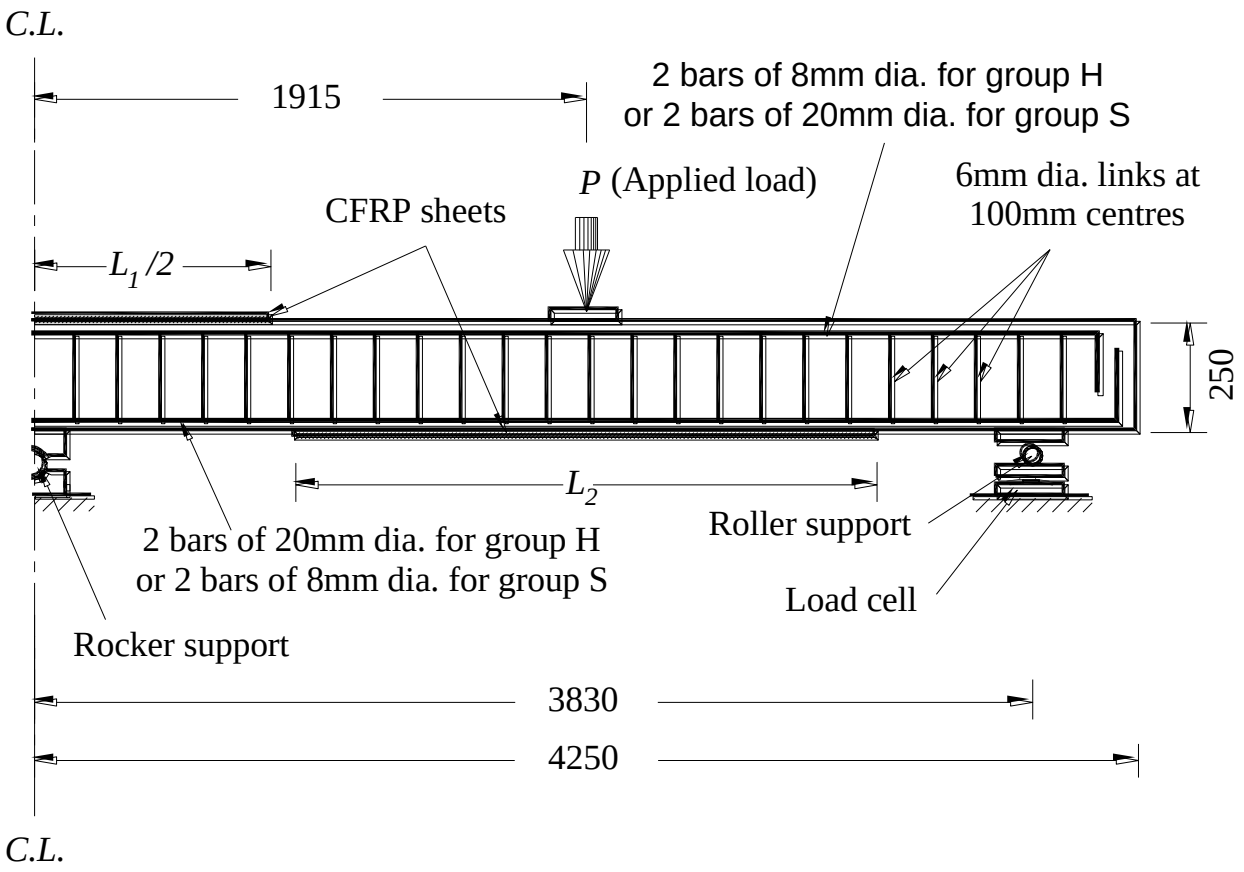


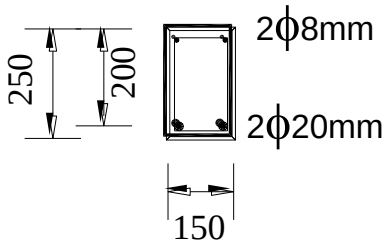


Typical cross section of beams in group H

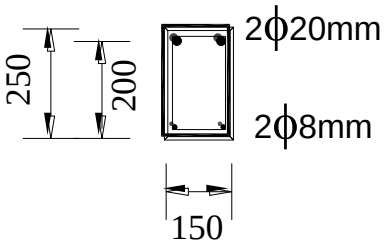


Typical cross section of beams in group S

Figure 1 Geometrical dimensions, reinforcement and test rig of test specimens

(all dimensions are in mm)


(a) Sagging flexural failure at mid-span

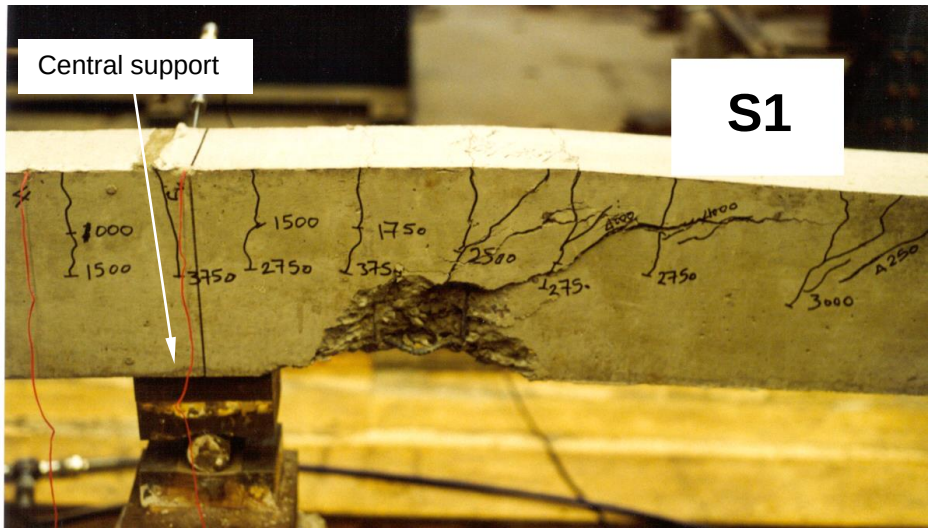


(b) Hogging flexural failure at the central support

Figure 2 Conventional ductile flexural failure of control beam S1

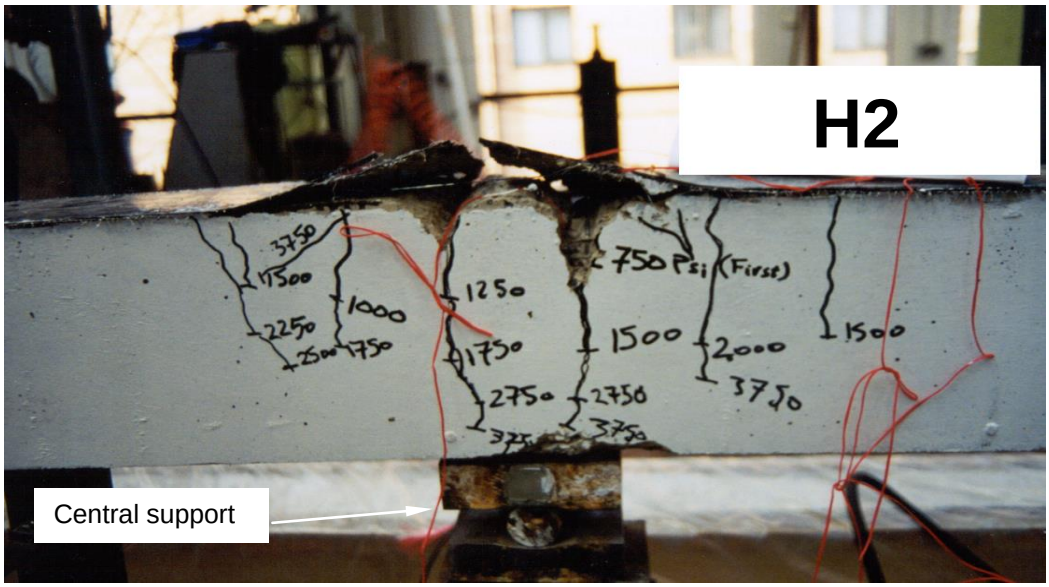


Figure 3 Tensile rupture of the CFRP sheets (beam H2)

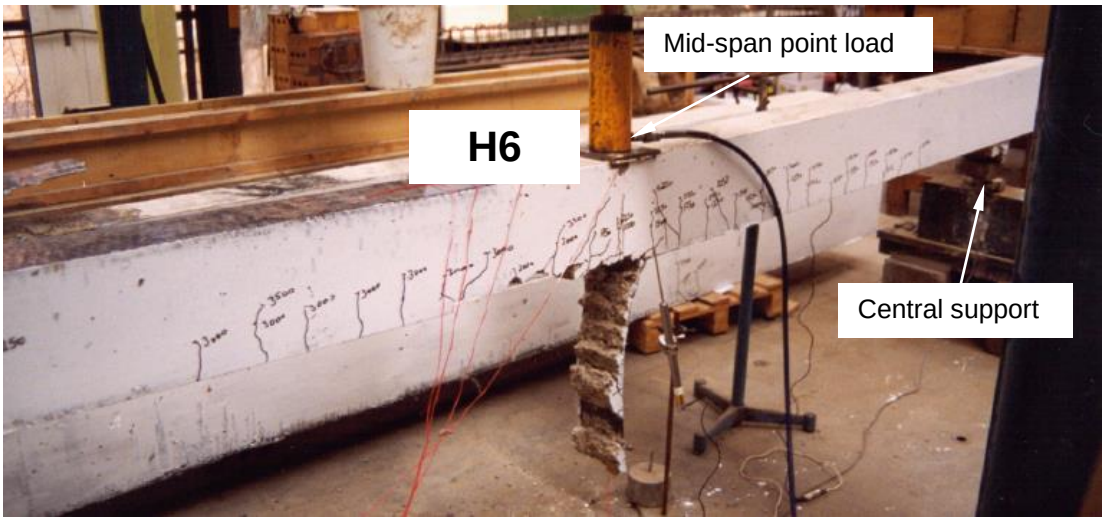


Figure 4 Peeling failure of the concrete cover initiated from the soffit CFRP sheet end near the central support (beam H6)

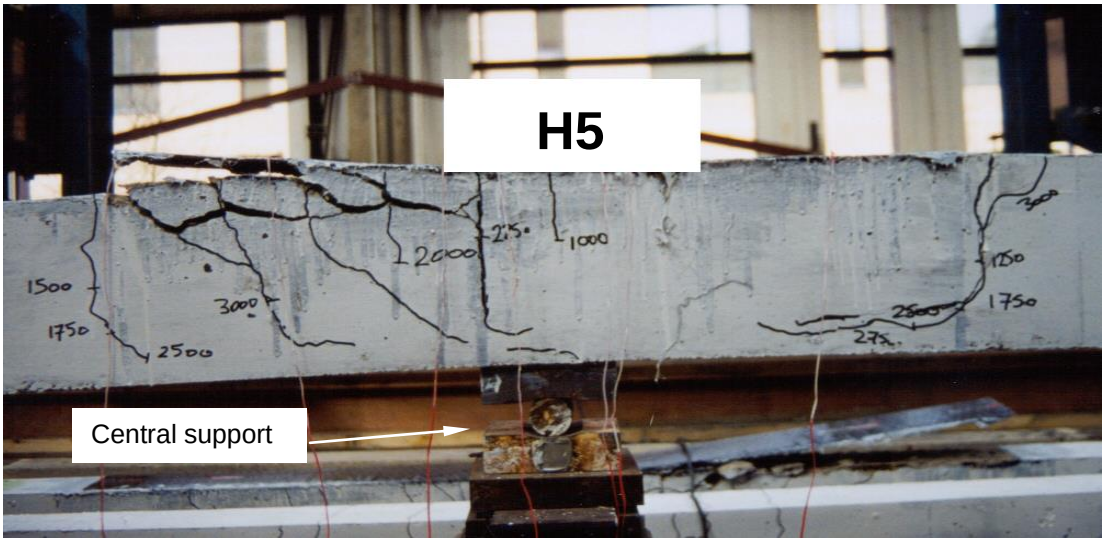


Figure 5 Peeling failure of the concrete cover initiated from the CFRP sheet end over the central support (beam H5)

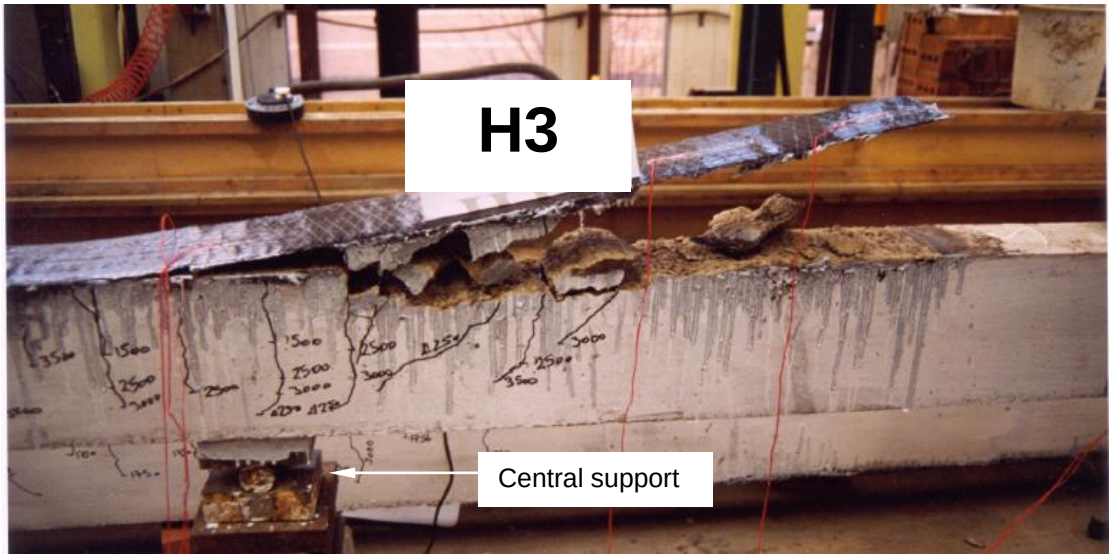


Figure 6 Peeling failure of the concrete cover over the central support away from the CFRP composite end (beam H3)

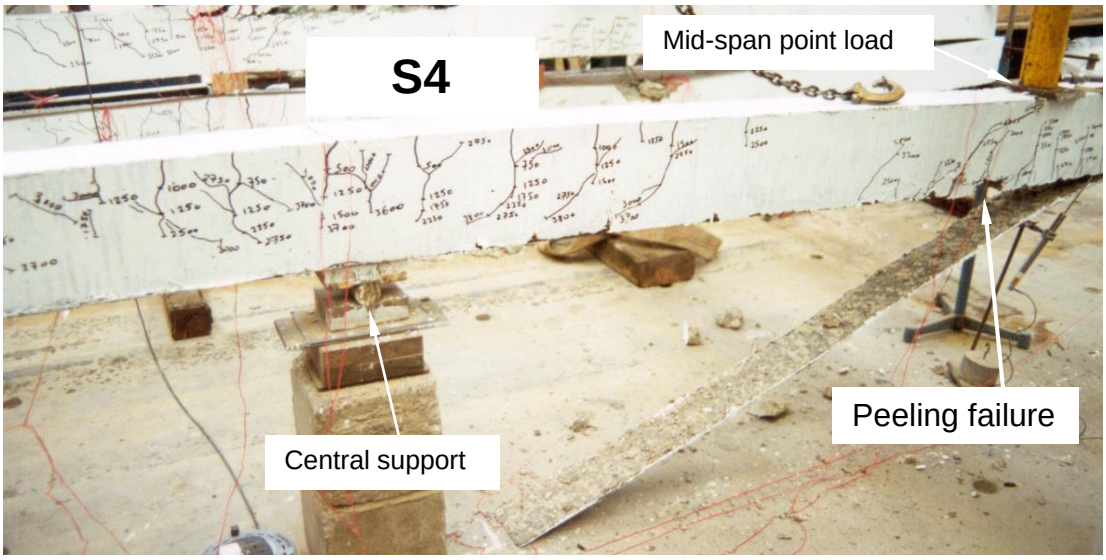


Figure 7 Peeling failure of the concrete cover under the point load away from CFRP sheet end (beam S4)

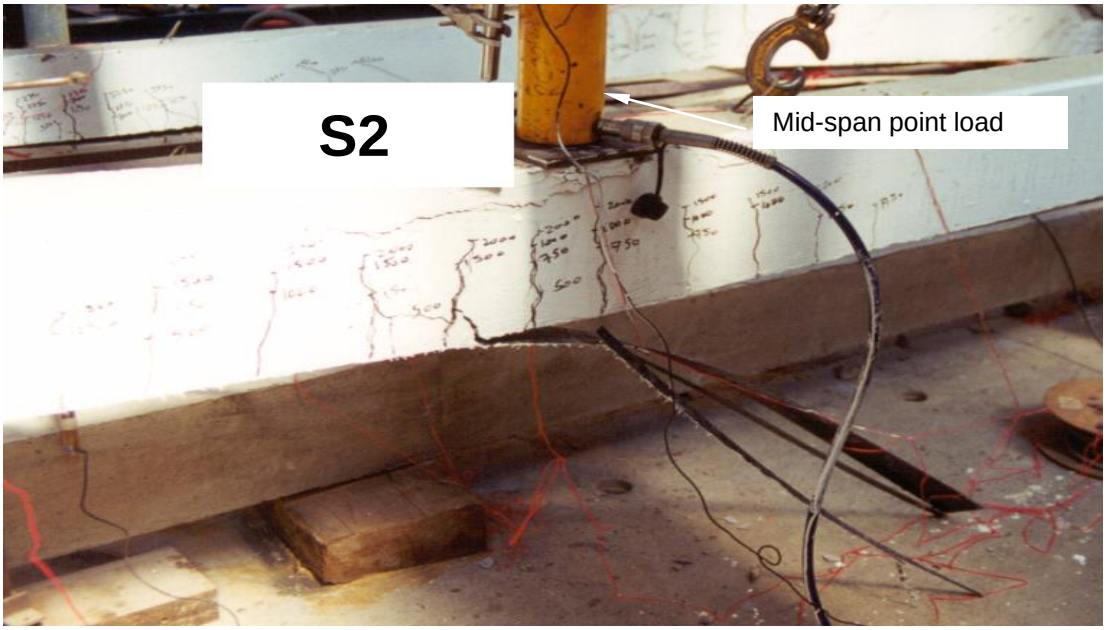


Figure 8 CFRP sheet separation from the beam soffit (beam S2)